New Journal of Physics
The open-access journal for physics

Organic layers at metal/electrolyte interfaces: molecular structure and reactivity of viologen monolayers

Stephan Breuer[1], Duc T Pham[1], Sascha Huemann[1], Knud Gentz[1], Caroline Zoerlein[1], Ralf Hunger[2], Klaus Wandelt[1,3] and Peter Broekmann[1]

[1] Institute of Physical and Theoretical Chemistry, University of Bonn, Wegelerstreet 14, 53115 Bonn, Germany
[2] Department of Material Science, Technical University of Darmstadt, Petersenstreet 43, 64484 Darmstadt, Germany
E-mail: k.wandelt@pc.uni-bonn.de

New Journal of Physics **10** (2008) 125033 (24pp)
Received 2 October 2008
Published 22 December 2008
Online at http://www.njp.org/
doi:10.1088/1367-2630/10/12/125033

Abstract. The adsorption of viologens (1,1′-disubstituted-4,4′-bipyridinium molecules) on a chloride-modified copper electrode has been studied using a combination of cyclic voltammetry (CV), *in-situ* scanning tunneling microscopy (STM) and *ex-situ* photoemission spectroscopy (XPS). Two prototypes of viologens could be identified with respect to their redox behavior upon adsorption, namely those which retain (non-reactive adsorption) and those which change their redox state (reactive adsorption) upon interaction with the chloride-modified copper surface at given potential. The first class of viologens represented by 1,1′-dibenzyl-4,4′-bipyridinium molecules (dibenzyl-viologens, abbreviated as DBV) can be adsorbed and stabilized on this electrode surface in their di-cationic state at potentials more positive than the reduction potential of the solution species. XPS N1s core level shifts verify that the adsorbed DBV molecules on the electrode are in their oxidized di-cationic state. Electrostatic attraction between the partially solvated viologen di-cations and the anionic chloride layer is discussed as the main driving force for the DBV stabilization on the electrode surface. Analysis of the N1s and O1s core level shifts points to a *non-reactive* DBV adsorption leaving the DBV^{2+}_{ads} solvation shell partly intact. The laterally ordered DBV^{2+}_{ads} monolayer turns out to be hydrophilic with

[3] Author to whom any correspondence should be addressed.

at least four water molecules per viologen present within this cationic organic film. The analysis of the Cl2p core level reveals that no further chloride species are present at the surface besides those which are specifically adsorbed, i.e. which are in direct contact with the metallic copper surface underneath the organic layer. The reduction of these adsorbed DBV^{2+}_{ads} surface species takes place only in the same potential regime where the solvated DBV^{2+}_{aq} bulk solution species react and is accompanied by a pronounced structural change from the di-cationic 'cavitand'-structure to a 'stripe'-structure of chains of π-stacked $DBV^{\bullet+}$ mono-cation radicals as verified by *in-situ* STM. The second class of viologens represented by 1,1′-diphenyl-4,4′-bipyridinium molecules (diphenyl-viologens, abbreviated as DPV) is much more reactive upon adsorption and cannot be stabilized on the electrode surface in a di-cationic state, at least within the narrow potential window of copper. The N1s core level binding energy indicates only the presence of the corresponding mono-reduced $DPV^{\bullet+}_{ads}$ species on the surface even at potentials more positive than the redox potential of the bulk solution species. This process leads to the formation of a hydrophobic viologen monolayer with stacked polymeric $\left(DPV^{\bullet+}_{ads}\right)_n$ chains as the characteristic structural motif. The *wet electrochemical reduction* of viologens is further compared with a *dry reduction* under UHV conditions. The latter reaction inevitably affects the di-cationic viologen species in the course of the photoemission experiment. Slow photoelectrons and secondary electrons are assumed to transform the di-cationic viologens into the corresponding radical mono-cations upon irradiation.

Contents

1. Introduction

Organic adsorbates play an important role in a number of electrochemical processes, e.g. as organic additives for metal plating. Furthermore, electrochemical deposition of thermally unstable molecules may also be a promising route towards functional organic layers. Detailed investigations are mandatory in order to acquire profound knowledge of the structural and electronic properties of these layers parallel and perpendicular to the surface, and to achieve a deeper mechanistic understanding of the kinetics of the involved charge transfer reactions taking place at the metal/organic interface in the electrochemical environment [1].

Detailed *in-situ* investigations of metal/electrolyte interfaces are becoming more and more possible with the same precision as known from ultrahigh vacuum surface science using scanning probe and photon-based methods. In particular, *in-situ* scanning tunneling microscopy (STM) has brought a considerable advancement of our understanding of electrified interfaces. In this context, the pioneering work of Siegenthaler and his group [2, 3] has to be emphasized that demonstrated the feasibility of electrochemical scanning tunneling microscopy (EC-STM) for the first time, and which allows the real space imaging of surfaces in contact with electrolytes and atomic resolution. By far, most of the EC-STM investigations since then have been performed under potentiostatic and equilibrium conditions. A particular experimental challenge, however, remains the characterization of the interface under reactive conditions, e.g. *during* an ongoing electron transfer reaction.

Interfacial redox reactions do not necessarily take place at the bare metallic electrode surface. Adsorbed anions from the supporting electrolyte can alter both the geometric and electronic structure of the electrode surface and, as a consequence, the charge distribution perpendicular to the surface in the entire near-surface electrolyte regime [4]. The impact of this anion adsorption on the kinetics of electrochemical reactions is well known from the early work of Frumkin [5]. The interfacial behavior becomes even more complex when reactants and/or products of the electron transfer process remain adsorbed on the anion-modified electrode surface prior to or during the reaction. Provided the anions retain to a large extent their negative charge upon specific adsorption, the subsequent adsorption of cationic reactants from the electrolyte onto the electrode surface will be facilitated through electrostatic attraction, thus, giving rise to the formation of 'paired'anion–cation layers [6]–[10], which remain stable even during an ongoing electron transfer reaction of the 'bulk' solution species [7, 11]. Such an anion–cation layering has recently been reported for the adsorption and subsequent reaction of redox-active viologens [12, 13] (1,1′-disubstituted-4,4′-bipyridinium molecules) on a chloride-modified Cu(100) electrode surface [7, 8, 10].

Di-cationic viologen species (V^{2+}) can reversibly be transformed into their corresponding radical mono-cations ($V^{\bullet+}$) via a one-electron transfer step:

$$V^{2+} + e^- \rightleftharpoons V^{\bullet+}. \tag{1}$$

This first electron transfer reaction can be followed by a subsequent dimerization or even an oligo- or polymerization of the formed radical mono-cations:

$$nV^{\bullet+} \rightleftharpoons (V^{\bullet+})_n. \tag{2}$$

Oligomeric and polymeric reaction products tend to accumulate directly at the electrode surface [7, 8], while the dimer species remains water soluble [12, 13].

A second single-electron transfer step transforms the radical mono-cation into a fully uncharged viologen species,

$$V^{\bullet+} + e^- \rightleftharpoons V^{o}. \tag{3}$$

The latter transition has to be considered as less reversible than the first electron transfer [12, 13].

Furthermore, the two sequential electron transfer steps in the viologen redox chemistry can interfere with an additional con-proportionation reaction between the uncharged and the di-cationic viologen species to the corresponding radical mono-cation as

$$V^0 + V^{2+} \rightleftharpoons 2V^{\bullet+}. \tag{4}$$

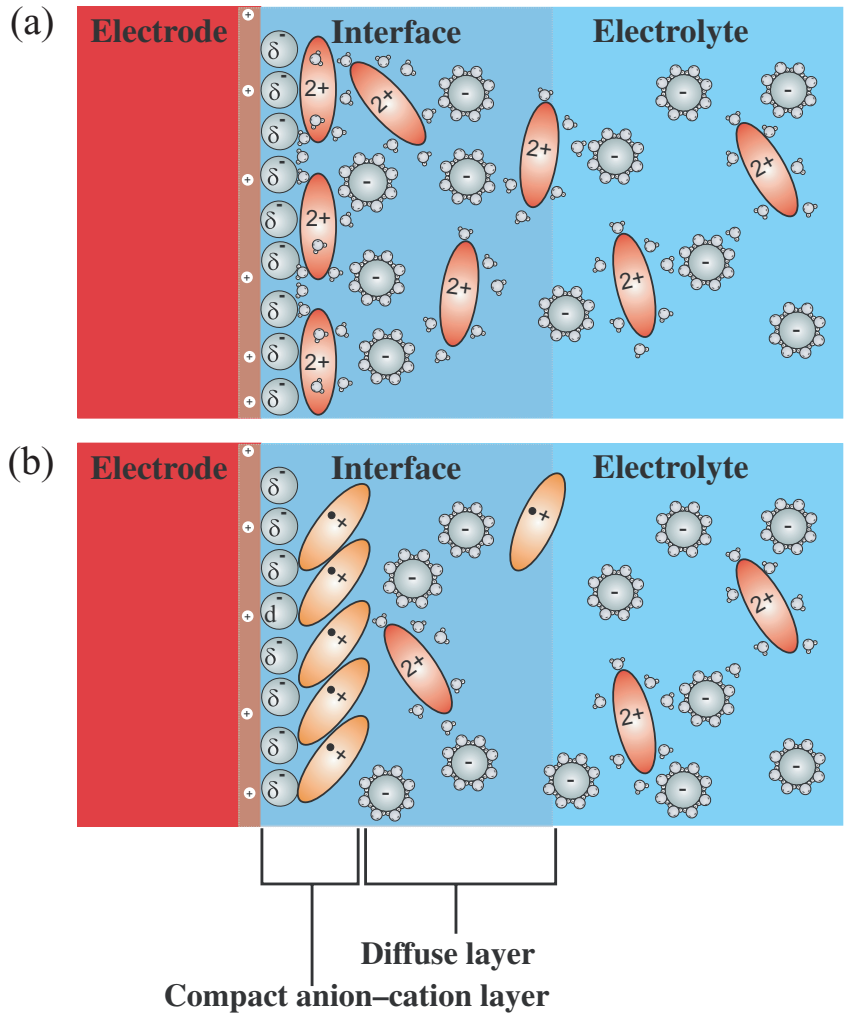

Figure 1. Schematic drawings showing the interfacial structure in the presence of redox-active viologens: (a) *hydrophilic* co-adsorption of di-cationic viologens and water on the halide-modified copper electrode; (b) compact *hydrophobic* stacking phase of mono-reduced viologens on the halide-modified electrode surface.

Depending on the solubility of the radical mono-cation, an insoluble precipitate can be formed as

$$n\mathrm{V}^{\bullet+} + \mathrm{nX}^{-} \rightleftharpoons \left(\mathrm{V}^{\bullet+}\mathrm{X}^{-}\right)_n \downarrow . \tag{5}$$

Figure 1(a) illustrates the layered arrangement of specifically adsorbed anions and redox-active viologens in their di-cationic state on an anion-modified electrode surface prior to the on-set of any electron transfer reaction [7, 8, 10]. Subsequent electron transfer reactions may lead to distinct 2D structural phase transitions within the viologen monolayer if the reaction product remains adsorbed; the underlying anion lattice usually remains unaffected by this process [7, 8, 10]. Adsorbed viologens often form more compact phases in their mono-reduced than in their di-cationic state [7, 8, 10]. While the ordering within the monolayer of mono-reduced viologens is dominated by intermolecular interactions (figure 1(b)) [7], that

of di-cationic viologen species is governed by electrostatic adsorbate–substrate interactions (figure 1(a)) [7, 8, 10].

In particular, when the reactants are pre-adsorbed on the electrode surface, the question naturally arises whether the adsorption process itself alters the reactivity of the *surface species* with respect to the corresponding *bulk solution species*. For instance, from viologens adsorbed on the basal plane of highly oriented pyrolytic graphite (HOPG), it is well known that characteristic spike-like 'pre-waves' appear in the voltammograms at potentials more positive than the main 'redox waves' [14, 15], [17]–[20]. These characteristic pre-peaks were first observed by Arihara *et al* [15] and later explained by Sagara's group in terms of Faradaic processes involving the pre-adsorbed viologen species [14, 17, 18]. A diluted 'gaseous' phase of adsorbed di-cationic viologens was assumed to transform into a more compact and condensed layer of mono-reduced viologens upon passing the spike-like pre-waves in the cyclic voltammogram pointing to a 'surface' reaction of viologens that takes place at potentials more positive than the reduction potential of the solution species. This phenomenon was reported not only for HOPG [14, 15], [17]–[20] but also for metallic mercury electrodes [21, 22].

The main focus of the present contribution lies in the correlation between the lateral order of the adsorbed viologen monolayers and their exact chemical composition, i.e. their redox state, right after the initial adsorption on the electrode surface. The discussion of this correlation, of course, has to consider the influence of possible counter-ion co-adsorption and solvation/de-solvation phenomena, which might be triggered by any ongoing electron transfer. Counter-ion co-adsorption and solvation effects are expected to be more important for the hydrophilic viologen di-cation phases than for the more hydrophobic films of mono-reduced viologens. In order to address these topics we employed *in-situ* STM and *ex-situ* photoelectron spectroscopy (XPS).

2. Experimental section

For all solutions, high-purity water (Milli-Q purification system; conductivity $< 18\,\mathrm{M\Omega\,cm}$; TOC $< 5\,\mathrm{ppb}$) and reagent grade chemicals were used. All electrolyte solutions were routinely deoxygenated with argon gas (5.0) for several hours before use. All potentials given in the text refer to a reversible hydrogen electrode (RHE), and a Pt-wire served as counter-electrode.

For the Cu(100) single crystal, a surface orientation of less than 0.5° off the (100) plane was required in order to guarantee a reproducibly smooth surface. Prior to each experiment, the copper surface needed to be etched in order to remove the native oxide film that is formed in air. Therefore, the sample was immersed into 50% orthophosphoric acid. Subsequently, an anodic potential of 2 V was applied between the copper electrode and a platinum foil for about 20–40 s. After etching the copper surface was rinsed with degassed 10 mM hydrochloric acid solution and mounted onto the electrochemical cell. All experiments routinely started with an electrochemical characterization of the Cu(100) surface in the pure supporting electrolyte (10 mM HCl). The working electrolyte (10 mM HCl + 0.1 mM $DBVCl_2$ or 10 mM HCl + 0.1 mM $DPVCl_2$) was introduced into the system under control of the potential in the regime between $E_{\mathrm{work}} = 0\,\mathrm{mV}$ and $E_{\mathrm{work}} = +100\,\mathrm{mV}$. All microscopic experiments have been performed using a home-built EC-STM. Further information about the STM set-up and the tip preparation can be found in the literature [23].

Additional photoemission studies were performed using the solid/liquid interface analysis system (SoLiAS) experimental station at the undulator beamline U49/2-PGM2 at the synchrotron light source BESSY II [16]. It allows high-resolution synchrotron photoelectron spectroscopy of electrochemically processed surfaces. Electrochemical processing was performed in an atmospheric pressure inert-gas cell using a classical hanging meniscus configuration followed by a transfer of the electrode surface into the vacuum via a purpose-designed load lock. Photoelectron spectra were obtained using a Phoibos 150 MCD 9 analyzer (SPECS). All spectra were recorded in normal emission and are referenced to the respective Fermi level of the metallic substrate. Thus, the displayed energy scales in the XPS spectra correspond to binding energies (BE). The total experimental resolution including the energy width of the photon beam and the detector resolution amounts to 100 meV. XPS data obtained from the solid di-chloride salts of the respective viologens, which were deposited on a clean gold foil under ambient conditions, served as references for the XPS spectra of the electrochemically processed surfaces.

3. Results and discussion

3.1. The substrate and the adsorbates

Figure 2 displays the surface morphology and atomic scale structure of the Cu(100) electrode exposed to the pure supporting electrolyte. In 10 mM HCl solution specifically adsorbed chloride anions form a $c(2 \times 2)$-Cl adlattice on Cu(100) [24] that is stable within the potential range between copper dissolution and the on-set of the hydrogen evolution reaction (HER). As known from the literature [4], [24]–[26] the presence of the chloride adlayer induces a preferential alignment of steps parallel to the substrate ⟨100⟩ directions along the close-packed chloride rows. This morphological feature serves as a safe indication for the presence of an intact chloride lattice with a chloride coverage close to saturation.

Recent *in-situ* surface x-ray scattering experiments indicate that chloride anions remain to a large extent negatively charged upon adsorption on Cu(100) [27]. This could be concluded from the huge interlayer spacing between the chloride lattice and the topmost copper layer of 0.196 nm and an outward relaxation of the topmost copper layer by 2.2% with respect to the respective bulk value of $d_{\mathrm{Cu–Cu}} = 0.181$ nm [27].

As often observed for condensed layers of specifically adsorbed anions also the chloride lattice on Cu(100) induces a charge reversal across the interface [7, 9, 10, 28]. This influences the electrostatic interactions that have to be considered as important driving forces for the adsorption of weakly solvated cationic species on the negatively charged chloride lattice (figure 1(a)) [7, 9, 10, 28].

The focus of this paper is on two particular viologens, the dibenzyl-viologen (1,1′-dibenzyl-4,4′-bipyridinium (DBV)) and the diphenyl-viologen (1,1′-diphenyl-4,4′-bipyridinium (DPV)). Their molecular structures are presented in figures 2(d) and (e). Note that the electron transfer affects the intramolecular viologen structure, in particular the central ‘bipy’ unit which tends to undergo a planarization in the course of the first electron transfer process [8, 12, 13].

The main difference between DBV and DPV consists of the extra methylene group separating the phenyl groups from the central bipy unit in case of the DBV, while for DPV the conjugated π-system extends over the entire molecule (figure 2(e)). In the following, it will be demonstrated that this small structural difference significantly affects both the viologen

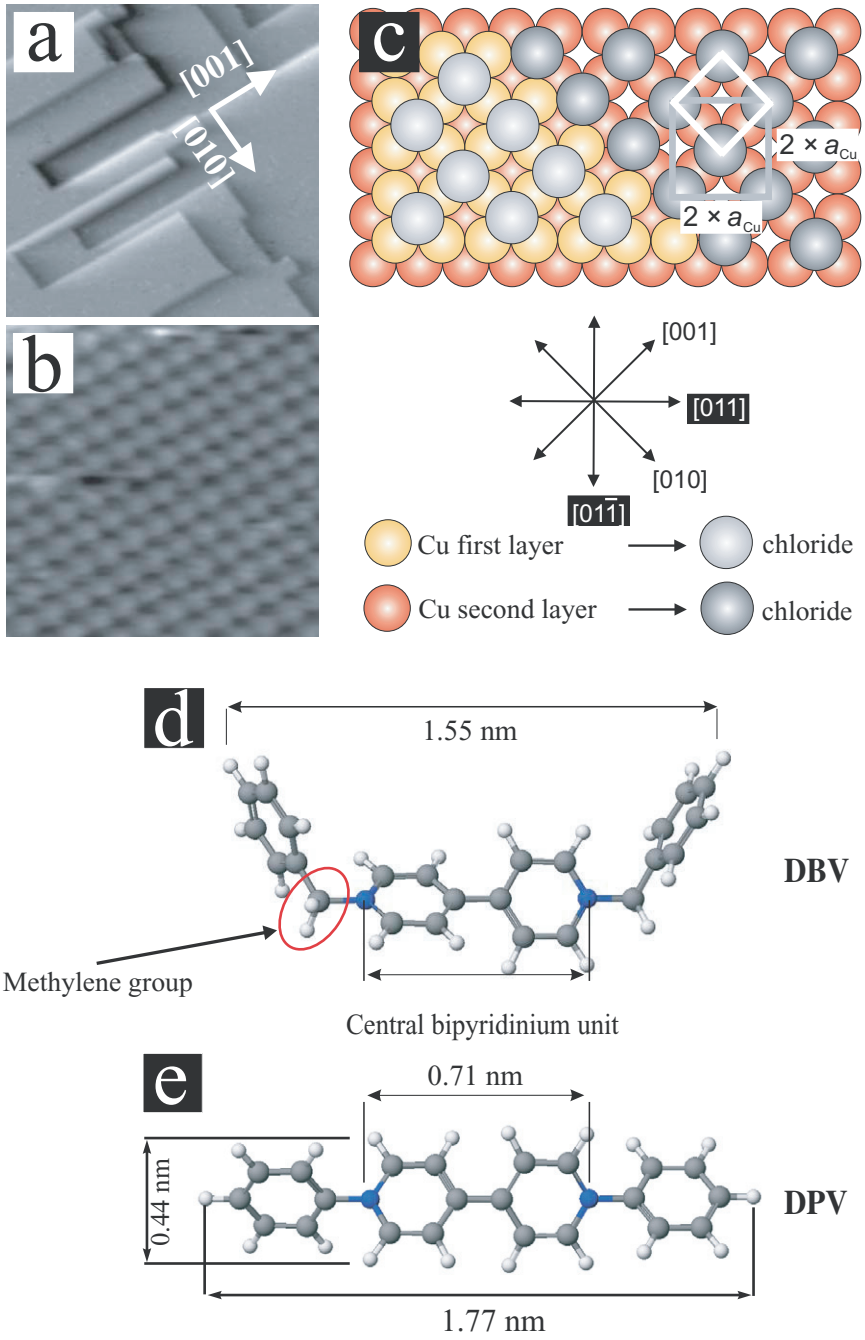

Figure 2. (a) Morphology of the Cu(100) electrode in the presence of the $c(2 \times 2)$-Cl layer, 87 nm × 87 nm, $I_t = 5$ nA, $U_b = 27$ mV, $E_{work} = +100$ mV versus RHE; (b) atomic structure of the $c(2 \times 2)$-Cl phase, 3.9 nm × 3.9 nm, $I_t = 5$ nA, $U_b = 25$ mV, $E_{work} = +100$ mV versus RHE; (c) molecular structure of the di-cationic DBV^{2+} (dibenzyl-viologen; 1,1′-dibenzyl-4,4′-bipyridinium); (d) molecular structure of the di-cationic DPV^{2+}(diphenyl-viologen; 1,1′-diphenyl-4,4′-bipyridinium).

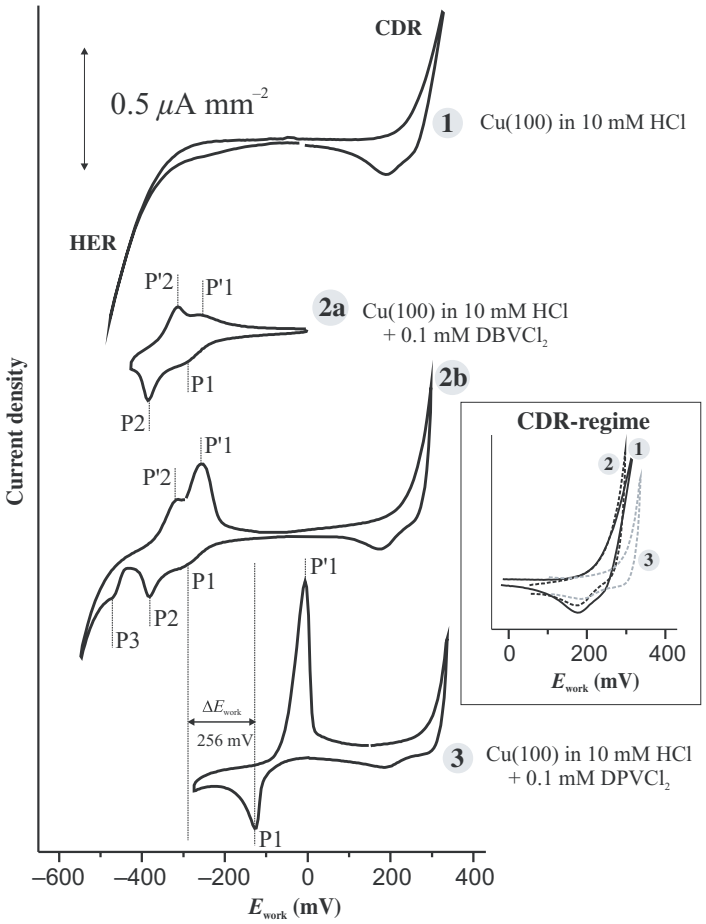

Figure 3. Overview of the electrochemical behavior of Cu(100) in the absence and presence of DBV and DPV.

solution redox chemistry and the structural phase behavior of the adsorbed viologen species. The fully conjugated π-system of the DPV can be expected to stabilize the radical mono-cation more effectively than the 'isolated' π-system of the central 'bipy'unit in the case of DBV.

3.2. Electrochemical characterization

Figure 3 displays the voltammetric behavior of Cu(100) in the absence (CV 1) and the presence (CVs 2 and 3) of viologens. CV 1 represents the standard CV of Cu(100) in pure 10 mM HCl solution revealing the narrow copper potential window, which is confined at the anodic limit by the copper dissolution reaction (CDR) and the corresponding re-deposition reaction in the reverse potential scan. At the cathodic limit, it is the on-set of the HER which confines the copper potential window. Changes in the voltammetric behavior due to the presence of DBV in the electrolyte are displayed in CV 2a. As long as we restrict the cathodic potential limit to $E_{\text{work}} > -400$ mV, we have to deal only with the first electron transfer step of the viologen redox system (equation (1)) that takes place close to the cathodic limit of the copper potential window [7]. On the basis of concentration depending CV measurements in combination with *in-situ* STM studies, we could clearly correlate peak system P1/P′1 with the first electron

transfer reaction involving both DBV^{2+}_{aq} di-cations from the 'bulk solution' and the adsorbed DBV^{2+}_{ads} 'surface' species. It should be noted that this electron transfer reaction does not occur on the bare metallic copper electrode but in the presence of a $c(2 \times 2)$ chloride adlayer, which is intact at least at potentials above peak system P2/P′2. For the reduction of the di-cationic DBV^{2+} species to the corresponding radical-mono cations there was no significant difference in reactivity observed between adsorbed DBV^{2+}_{ads} 'surface' and the respective DBV^{2+}_{aq} 'solution' species [7]. A continued reduction of di-cationic bulk solution species to the corresponding mono-cationic species takes place in the presence of both the compact layer of stacked radical mono-cations and the chloride lattice underneath (figure 1(b)) [8].

Peak system P2/P′2 could be attributed to the (quasi)reversible desorption/re-adsorption of chloride anions through the viologen film being accompanied by a disorder/order phase transition within the 2D monolayer of mono-reduced $DBV^{\bullet+}_{ads}$ species [8].

A further decrease of the cathodic potential limit in the CV to $E_{work} = -480\,mV$ initiates the second DBV electron transfer reaction (see CV 2b and equation (2)). This process can be correlated with P3 at $E_{work} = -440\,mV$ (cathodic sweep) that is already superimposed on the starting HER. Compared with the pure supporting electrolyte (CV 1 in figure 2) the on-set of the HER is significantly shifted to lower potentials when DBV is present in the electrolyte (CV 2b in figure 2) pointing to adsorbed reduced viologen species blocking reactive sites for the HER. The current features in the corresponding anodic potential sweep appear more complex. A distinct oxidation peak P′3 that corresponds to P3 is missing in the reverse potential scan. This effect might be related to the viologen con-proportionation reaction transforming the uncharged DBV^{0} that appears at potentials below $E_{work} = -440\,mV$ and the di-cationic DBV^{2+}solution species to the corresponding radical mono-cationic $DBV^{\bullet+}$ species according to equation (4) [12, 13]. As a consequence P′1 is significantly larger in CV 2b than in CV 2a.

From a comparison of CV 2a and 3, it becomes obvious that DPV is electrochemically more reactive than DBV. Therefore, all viologen-related redox processes are shifted to higher potentials compared with those of the DBVs. The first reduction peak P1 already appears at $E_{work} = -128\,mV$ with a resulting difference of $\Delta E_{work} = +256\,mV$ between P1(DBV) and P1(DPV). P′1 in the reverse scan of CV 3 corresponds to the re-oxidation of the $DPV^{\bullet+}$ species to the corresponding water-soluble DPV^{2+} species.

A further difference between the DPV- and the DBV/Cl/Cu(100) system concerns the onset of the CDR. The inset in figure 3 represents the anodic potential regime of all three CVs. While there is no significant difference in the dissolution kinetics of Cu(100) in the pure supporting and the DBV containing electrolyte, we observe an upward shift of the CDR to higher potentials when DPV is present. It can be assumed that the adsorbed DPV effectively blocks reaction sites for the copper dissolution process, e.g. step edges, thereby causing the observed inhibition effect.

The differences observed in the DBV and DPV redox chemistry find their correspondence also in related surface structure transitions. In order to illustrate this, we focus in the following on the different adsorption behavior of DBV and DPV at potentials above the main redox waves.

3.3. In-situ STM results

Figure 4 provides an overview of the 2D structures of the respective viologen films adsorbed on the $c(2 \times 2)$-Cl adlattice on the Cu(100) surface. Adsorbing DBV under *non-reactive conditions* on $c(2 \times 2)$-Cl at potentials above P1/P′1 leads to the formation of a laterally

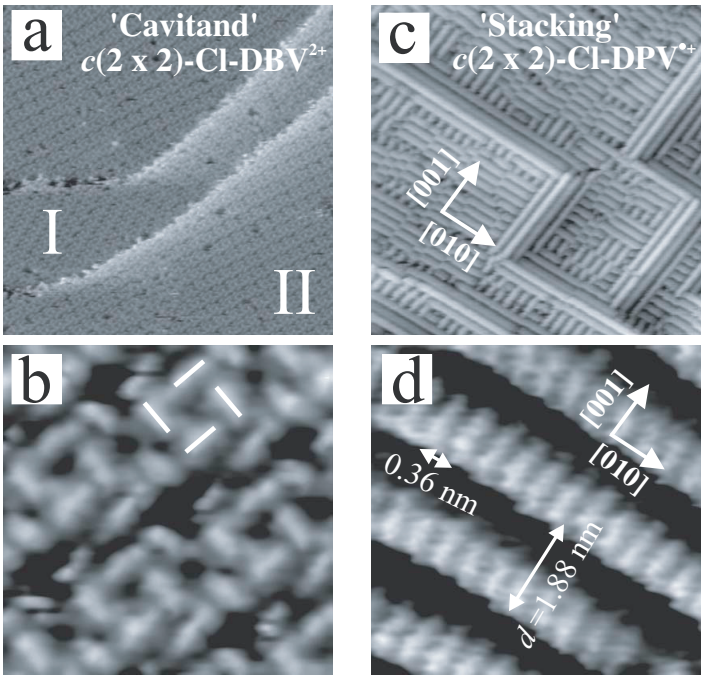

Figure 4. Overview of the DBV and DPV phases on the chloride-modified Cu(100) surface at high potentials. (a)–(b) DBV^{2+}_{ads} on Cu(100)-$c(2 \times 2)$-Cl; (a) 54.5 nm × 54.5 nm, $I_t = 1.1$ nA, $U_b = 350$ mV, $E_{work} = -190$ mV; (b) 7.8 nm × 7.8 nm, $I_t = 1.1$ nA, $U_b = 350$ mV, $E_{work} = -150$ mV; (c)–(d), $DPV^{\bullet+}_{ads}$ on Cu(100)-$c(2 \times 2)$-Cl; (c) 57.6 nm × 57.6 nm, $I_t = 0.6$ nA, $U_b = 250$ mV, $E_{work} = 0$ mV; (d) 4.1 nm × 4.1 nm, $I_t = 5.0$ nA, $U_b = 350$ mV.

well-ordered organic layer consisting of di-cationic DBV^{2+}_{ads} species (figures 4(a) and (b)), [7]–[10], [28]. A chiral 'cavitand'-like assembly of 4 DBV^{2+}_{ads} entities (white lines in figure 4(b)) has been identified as the key structural motif of this viologen adlayer occurring in two mirror domains. One can describe this viologen structure by a transformation matrix

$$\begin{pmatrix} a_{vio} \\ b_{vio} \end{pmatrix} = \begin{pmatrix} 2 & 7 \\ \overline{7} & 2 \end{pmatrix} \begin{pmatrix} a_{Cl} \\ b_{Cl} \end{pmatrix}$$

relating the viologen layer to the underlying $c(2 \times 2)$-Cl lattice or alternatively by

$$\begin{pmatrix} a_{vio} \\ b_{vio} \end{pmatrix} = \begin{pmatrix} 5 & 9 \\ \overline{9} & 5 \end{pmatrix} \begin{pmatrix} a_{Cu} \\ b_{Cu} \end{pmatrix}$$

relating the viologen lattice directly to the copper substrate [7]–[10], [28]. Lattice vectors of the DBV^{2+}_{ads} film amount to $|\vec{a}| = |\vec{b}| = 2.6 \pm 0.02$ nm enclosing an angle of $90^\circ \pm 2^\circ$. Apart from this 'cavitand'-like structure motif there are further satellite spots in the STM image visible which, however, appear only under certain tunneling conditions. Their origin is still under discussion. One reasonable explanation assumes further adsorbed DBV^{2+}_{ads} species residing in different adsorption sites and geometries than those constituting the 'cavitand' ensemble. An alternative interpretation assuming a further co-adsorption of anions and/or water molecules within the viologen layer as origin of the satellite spots in the STM experiment, however, will

be discussed in more detail at the end of this work. As we will show, the co-adsorption of anions can be ruled out. A preliminary structure model has been discussed in detail elsewhere [7, 8, 10, 28].

It has been reported [7, 10, 28] that the DBV^{2+}_{ads} film undergoes a structural transition when reaching the redox-system P1/P′1 pointing to a phase transition triggered by the starting electron transfer reaction from the DBV^{2+}_{ads} di-cations to the corresponding $DBV^{\bullet+}_{ads}$ radical mono-cations. The surface confined product of this reaction is a stripe phase of polymerically stacked radical mono-cations (similar to figure 4(d)) that self-assembles into several rotational and mirror domains [7, 10, 28]. It could be shown that the electron transfer reaction of viologen molecules from solution goes on even in the presence of the $(DBV^{\bullet+}_{ads})_n$ stacking phase [7].

The DBV and DPV monolayer phases which are present on Cu(100) at potentials *more positive than the main redox waves* in the CV differ significantly in their structural appearance (see figures 4(a), (b) and (c), (d)), in that DPV adsorption leads exclusively to a stacking phase (figures 4(c) and (d)). This observation appears surprising since this stacking motif has been identified as a structural 'fingerprint' for the presence of mono-reduced viologen species but not for the presence of adsorbed viologens in their di-cationic redox state [7, 10, 28].

The DPV stacking chains are preferentially oriented along the substrate ⟨100⟩ directions. The alignment of substrate steps along the ⟨100⟩ directions is clearly indicative for the presence of the $c(2 \times 2)$-Cl underneath (see figure 2(a)). It is worth mentioning that the lateral order of the DPV stacking phase is particularly well developed close to the mono-atomically high substrate steps. This results in two almost defect-free stacking chains running parallel on either side of these step edges, i.e. the upper and the lower side. The specific affinity of DPV towards substrate step edges can further be demonstrated by using low concentration DPV solutions (figure 5). Under these experimental conditions no condensation and lateral ordering of DPV is observed on terraces. Only step edges that are oriented parallel to the substrate ⟨100⟩ directions are *selectively* decorated by DPV stacking chains (see white arrows '1' in figure 5), while step edges oriented along other crystallographic directions, e.g. ⟨110⟩, remain uncovered in this initial stage of the DPV phase formation (see white arrows denoted by '2' in figure 5). Each DPV chain in contact with a substrate ⟨100⟩ step contains DPV molecules that are oriented with their main molecular N–N axis perpendicular to the respective step edge and are therefore parallel to one of the ⟨100⟩ directions. There is a clear preference of DPV for the lower sites at step edges which become decorated first before the corresponding upper sites of the step edges are populated (figure 5). The observed preference of the adsorbed DPV molecules for the substrate steps explains the inhibiting effect of DPV on the copper dissolution and re-deposition reaction as revealed by the voltammetry (inset of figure 3). In full agreement with this reasoning is the observation that the 'cavitand' structure of di-cationic DBV species, though perfectly ordered on extended terraces but not aligned parallel to the steps, reveals a large number of defects at step edges, which cause the di-cationic DBV phase to have almost no inhibiting effect on the CDR [10, 28].

Due to symmetry reasons the DPV stacking phase occurs in two rotational domains rotated by 90°. The nearest neighbor distance (NND) of DPV entities within these stacking chains amounts to $NND_{DPV} = 0.36(2)$ nm which is identical to the NND of the underlying chloride lattice of $NND_{c(2\times2)\text{-Cl}} = 0.362$ nm and close to the intermolecular spacings of mono-reduced DBV species on both the $c(2 \times 2)$-Cl/Cu(100) surface and the chloride-free HOPG [7]. Therefore, we propose a structure model that assumes DPV entities adsorbed in a so-called

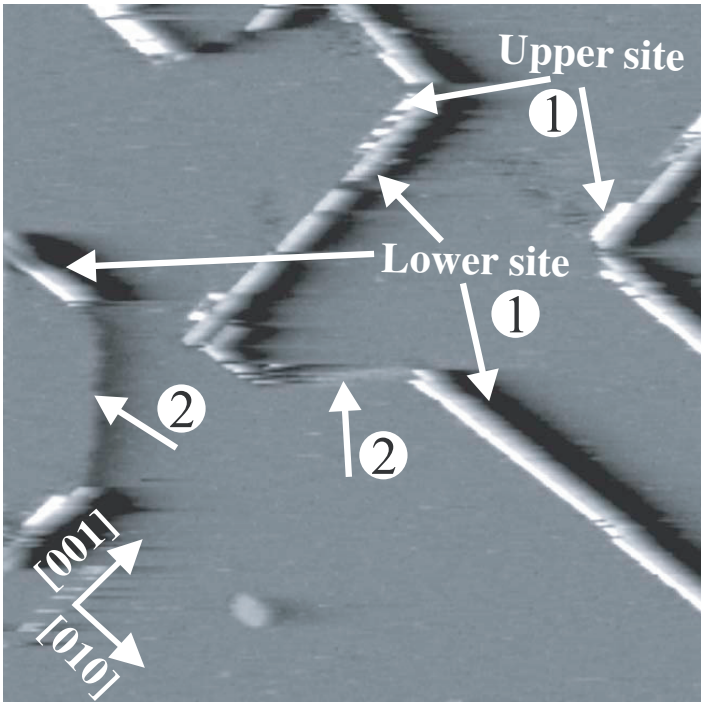

Figure 5. Selective decoration of ⟨100⟩ steps in the DPV submonolayer regime, 101 nm × 101 nm, $I_t = 0.1$ nA, $U_b = 350$ mV, $E_{work} = -150$ mV. The actual $DPVCl_2$ solution concentration was about $c(DPVCl_2) = 10^{-6}$ mol l^{-1}.

'edge-on' geometry with the molecular N–N-axes parallel to the surface (figure 6). It can further be assumed that the redox-active bipy groups are imaged brighter in the STM experiment than the phenyl groups which are most likely located within the 'darker grooves' of the stacking phase (figure 4(d)). The inter-chain distance amounts to $d = 1.88(2)$ nm and compares well with the length of the DPV molecules (figure 2(e)). An interdigitation of the phenyl groups of DPV entities into adjacent DPV stacking chains can therefore be ruled out. However, from the STM images alone it cannot be concluded whether the aromatic rings of the central 'bipy' unit are oriented perfectly perpendicular to the surface or whether the plane of the 'bipy' unit is slightly tilted.

Not only are the structural motifs different for the adsorbed DBV and DPV at high potentials (figure 4), but the potential dependence of the respective monolayer phases also reveals distinct differences. While the di-cationic DBV^{2+}_{ads} phase undergoes a phase transition upon passing P1 (figure 3, CV 2) resulting in a compact stacking phase similar to the one we observe for DPV already at high potentials there are no structural transitions within the observed DPV stacking phase when the main reduction peak P1 is passed (CV 3 in figure 3). Figure 7 shows a selection of such a potential-dependent series of STM images. The DPV stacking phase remains structurally intact even at $E_{work} = -310$ mV (figure 7(c)). The only effect of the potential on the DPV stacking phase consists in the appearance of small 'dots' within the darker grooves (inset of figure 7(c)). Note that the electrode surface is already under reactive conditions at these negative potentials (see figure 3, 2(b)). It can therefore be assumed that products of the 'bulk' solution reduction precipitate onto the stacking phase which, however,

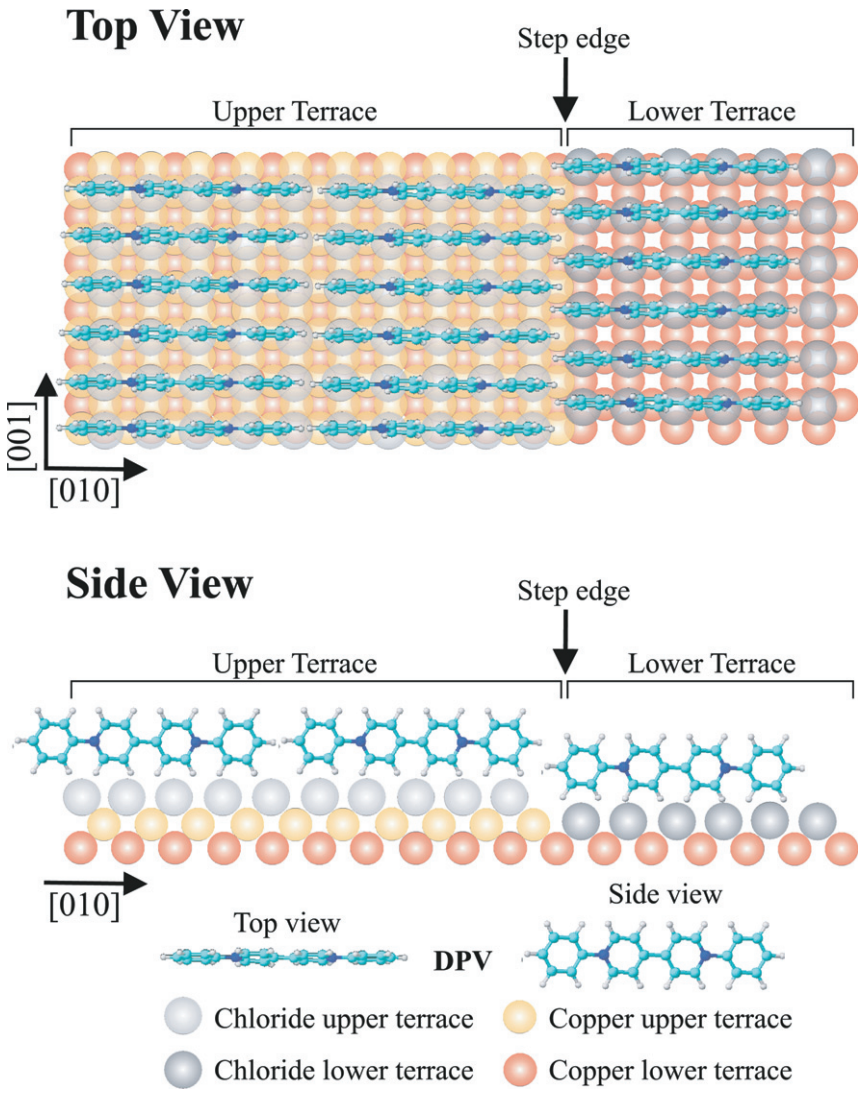

Figure 6. Preliminary structure model of the $(DPV^{\bullet+}_{ads})_n$ stacking phase on the Cu(100)-$c(2 \times 2)$-Cl layer.

are easily removed by the tunneling tip during scanning. Ongoing scanning at these negative potentials finally becomes hampered by the formation of a thick film of mono-reduced DPV species.

In the following, we exclusively focus on the chemical nature of the viologen monolayers at potentials *above* the main redox waves.

3.4. Ex-situ XPS results

Of particular interest is the chemical shift of the N1s emission which is sensitive to the redox state of the adsorbed viologen species. Note that the interpretation of the obtained XPS data relies on the assumption that the chemical composition of the interface and, in particular, the viologen redox state remains unaltered upon emersion of the electrode out of the electrochemical environment. This assumption, however, appears very much justified in the

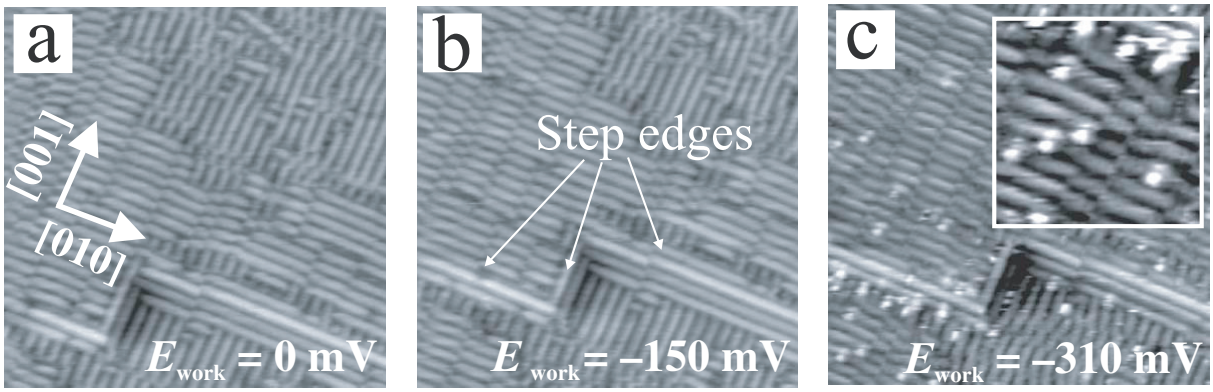

Figure 7. Potential-dependent series of STM images showing the structural stability of the $(DPV^{\bullet+}_{ads})_n$ stacking phase at potentials above and below the main reduction waves in CV3 of figure 3: (a)–(c) 50 nm × 50 nm, $I_t = 0.2$ nA, $U_b =$ 300 mV, the in-set in (c) represents an enlargement of (c) showing the preferred second-layer adsorption of reduced DPV species in the 'darker' grooves of the $(DPV^{\bullet+}_{ads})_n$ monolayer phase.

light of the results shown in figures 8–10 and their consistency with the electrochemical behavior discussed above.

The main question to be answered by the photoemission experiment is whether DPV exists in its di-cationic form on the chloride-modified copper surface at high potentials or whether it gets instantaneously reduced to the corresponding radical mono-cations even at potentials where the DPV^{2+}_{aq} solution species is still stable. Both the structural motif of the DPV phase at high potentials above the main reduction peak in the CV and the missing phase transition upon reaching P1 described above point to an instantaneous reduction of the di-cationic DPV^{2+} to the respective radical mono-cations upon adsorption. A similar phenomenon has been reported for various di-alkylated viologens adsorbed on HOPG [14], [17]–[19] or Hg [21, 22] electrodes, where spike-like pre-peaks appear in the CVs at potentials more positive than the corresponding main redox waves. Their origin was explained in terms of faradaic processes involving the surface-confined viologen species coupled with surface phase transitions transforming 'expanded' phases of viologen di-cations into more compact phases of the corresponding radical mono-cations at potentials above the main redox waves [17]–[20]. In accordance with the structural differences between adsorbed DBV and DPV seen in the *in-situ* STM experiments (figures 4 and 7) we, indeed, observe significant differences in the *ex-situ* photoemission experiment.

Figure 8(a) represents the N1s photoemission spectrum obtained from the DBV^{2+}_{ads} 'cavitand' layer (figure 4(a)) emersed out of the electrolyte at $E_{emers} = +100$ mV. The best fit was obtained assuming three individual viologen species with their main N1s component at $BE_1 = 402.10(2)$ eV and two further components at the lower binding energies $BE_2 =$ 400.08(2) eV and $BE_3 = 399.09(2)$ eV, respectively. These latter components have to be assigned to reduced viologen species. Similar multi-component N1s spectra were reported for various solid di-chloride salts of viologens. For instance, Liu *et al* [29] assign the main peak in their N1s spectrum of 1,1′-bis(4-vinyl-benzyl)-viologen at BE = 401.7 eV to the positively charged nitrogen of the viologen species (V^{2+}), a satellite feature at BE = 399.5 eV to the

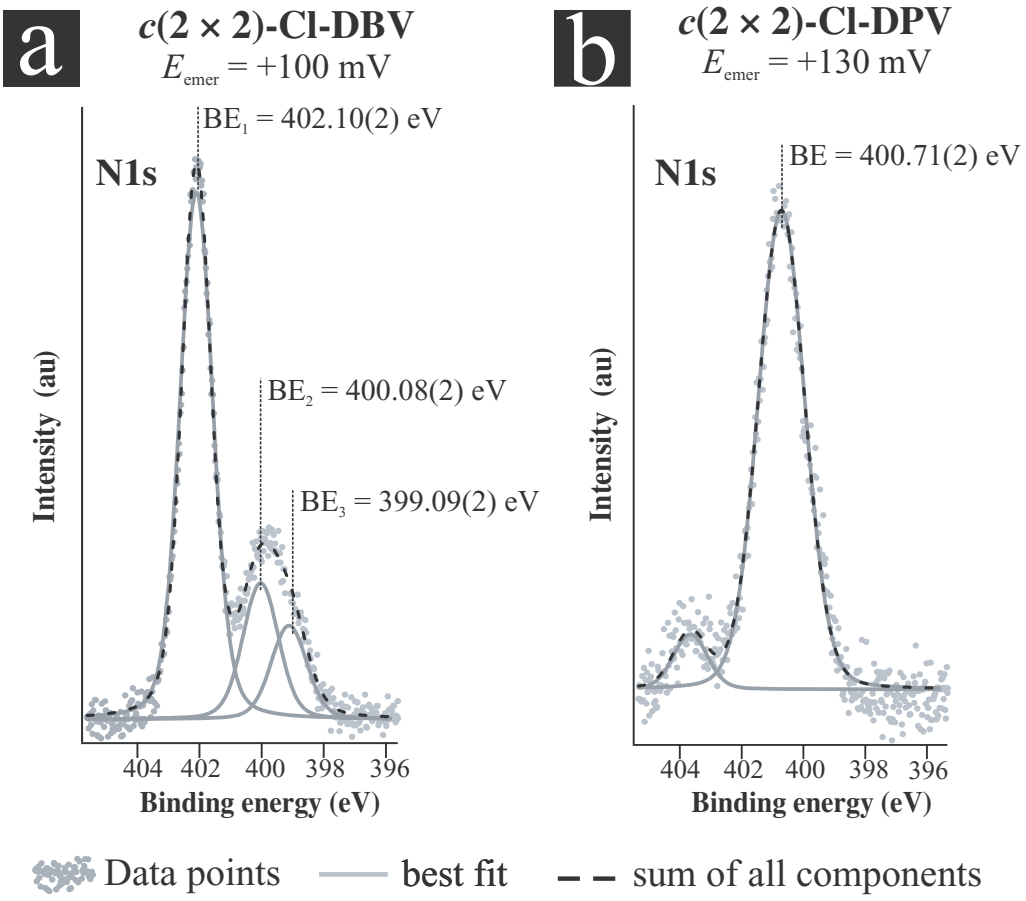

Figure 8. (a) N1s photoemission spectrum of the DBV^{2+}_{ads} monolayer phase, $E_{photon} = 720\,eV$, $E_{emers} = +100\,mV$; (b) N1s photoemission spectrum of the $(DPV^{\bullet+}_{ads})_n$ monolayer phase, $E_{photon} = 720\,eV$, $E_{emers} = +130\,mV$ (E_{emers} indicates the emersion potential where the copper sample was transferred from the electrochemical environment into UHV).

mono-reduced species ($V^{+\bullet}$) and a further satellite at even lower binding energy BE = 398.6 eV to the fully uncharged viologen (V^0). The presence of reduced viologen species in the viologen di-chloride salt has been rationalized in terms of an instability of the di-cationic viologen species against irradiation with x-rays. It appears most likely that such a transformation of di-cationic into the corresponding reduced viologen species is caused by slow photoelectrons and secondary electrons interacting with the di-cationic viologens which act as strong electron acceptors. In this respect, one could call this slow transformation a 'dry' reduction of di-cationic viologens under UHV conditions.

According to the reasoning in our previous papers we do not expect any reduced DBV species present at the electrode at these high potentials of $E_{work} = +100\,mV$ and therefore assign the main peak at $BE_1 = 402.10(2)\,eV$ to di-cationic DBV. It is most likely that the satellite peaks observed in the N1s spectrum (figure 8(a)) are also experimental artifacts due to the transformation of the *adsorbed* di-cationic to the corresponding mono-reduced viologen species upon irradiation as suggested by Liu *et al* for the 1,1′-bis(4-vinyl-benzyl)-viologen

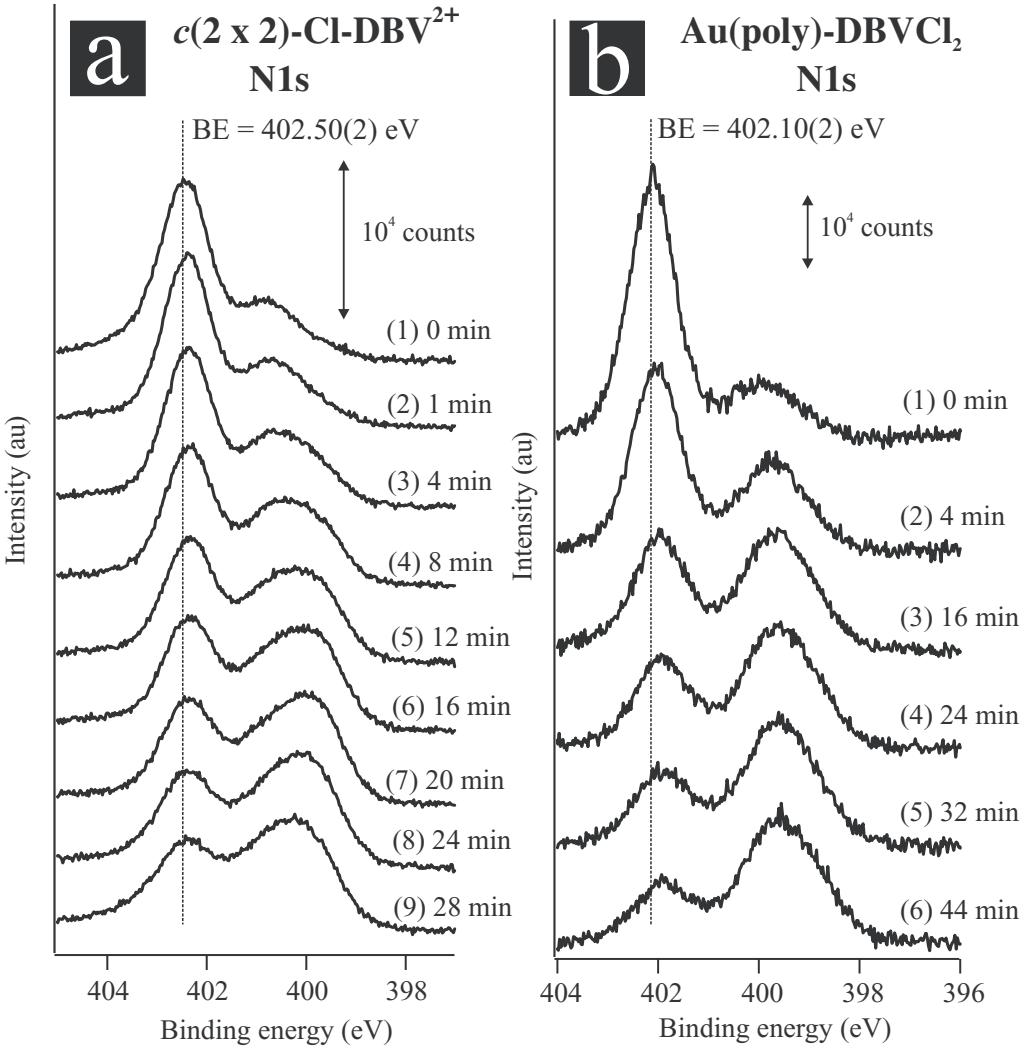

Figure 9. (a) Time-dependent N1s photoemission spectra of the DBV^{2+}_{ads} monolayer phase adsorbed on the chloride-modified copper electrode, $E_{photon} = 720\,eV$, $E_{emers} = +100\,mV$; (b) time dependent N1s photoemission spectra of the $DBVCl_2$ salt deposited on an inert gold foil.

di-chloride salt [29]. This hypothesis becomes experimentally substantiated by our time-dependent XPS measurements of the emersed DBV^{2+}_{ads} monolayer (figure 9(a)) and of the corresponding $DBVCl_2$ salt deposited on an inert gold foil (figure 9(b)). The latter is to serve as reference for the identification of the DBV in its di-cationic state on the chloride-modified surface at high potentials. We find the di-cationic DBV^{2+} in the di-chloride salt with an N1s binding energy of BE = 402.5 eV (figure 9(b)) which is slightly higher (0.4 eV) than the value observed for the adsorbed DBV^{2+}_{ads} (figure 8(a)). Both spectra show the same time dependence upon irradiation. While the main component decreases with irradiation time we observe an increase of the satellite peaks at lower BE which are attributed to the reduced DBV species (figure 9). Note, however, that the satellite features are already present in the first spectrum of a time-dependent XPS series (spectra at $t = 0\,min$ in figure 9). From these

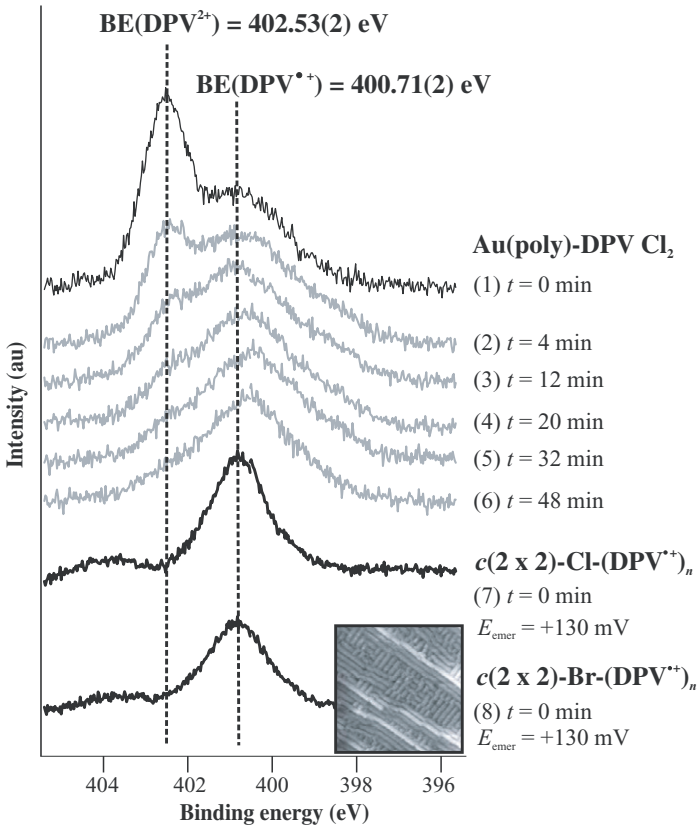

Figure 10. Time-dependent N1s photoemission spectra of the $DPVCl_2$ salt deposited on an inert gold foil compared with the N1s photoemission spectra obtained from the DPV monolayer phases on $c(2 \times 2)$-Cl and (2×2)-Br at high potentials, $E_{photon} = 720\,eV$.

observations we conclude that the DBV-'cavitand' layer (figures 4(a) and (b)) observed at potentials more positive than the main reduction wave indeed contains di-cationic DBV^{2+}_{ads} species in full agreement with our previous studies [8]–[10], [28].

Interestingly, the N1s emission of the DPV layer (figures 4(c) and (d)) emersed at similarly high potentials above the respective main reduction peak in the CV ($E_{emer} = +130\,mV$) behaves significantly different than the one of the DBV^{2+}_{ads} monolayer. The dominant N1s emission at $BE = 400.71(2)$ in figure 8(b) points to the presence of reduced $DPV^{\bullet+}_{ads}$ species at the electrode surface although DPV^{2+}_{aq} *solution* species are stable in their di-cationic form at these high electrode potentials (figure 3). Our assignment of the main N1s peak in figure 8(b) to the mono-reduced $DPV^{\bullet+}_{ads}$ species is clearly supported by measurements on the N1s binding energy of the di-cationic DPV^{2+} species in solid $DPVCl_2$ salt (figure 10). The latter was also deposited on an inert Au foil as the $DBVCl_2$ salt before. As expected, we found di-cationic DPV^{2+} at high binding energies of $BE = 402.53(2)$ eV (see XPS spectrum (1) in figure 10) as the main component. A similar BE was obtained for the di-cationic DBV^{2+} in the respective di-chloride salt with $BE = 402.10(2)$ eV (see XPS spectrum (1) in figure 9(b)). Similar to the DBV^{2+} in the $DBVCl_2$ salt also the DPV^{2+} suffers reduction upon irradiation. In line with the disappearance of the di-cationic DPV^{2+} species a broad satellite feature emerges

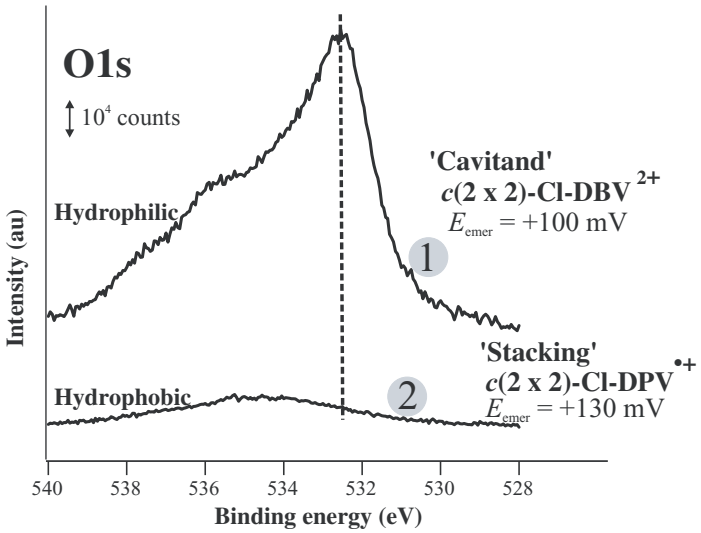

Figure 11. Overview of the O1s photoemission spectra of the viologen-covered Cu(100)-$c(2 \times 2)$-Cl phase, $E_{\text{photon}} = 720$ eV.

with time in the N1s photoemission spectrum also around the value as in the adsorbed case, i.e. BE = 400.71(2) eV, representing reduced DPV species as reaction products of the 'dry' DPV reduction. The emergence of this reduced DPV species again serves as reference for the identification of the mono-reduced $DPV^{\bullet+}_{ads}$ species on the halide-modified copper surface. For comparison we have included the N1s spectrum from figure 8(b) obtained for the DPV film on the chloride-modified copper in figure 10 (spectrum 7). Interestingly, we observe the reduced $DPV^{\bullet+}_{ads}$ species not only on the $c(2 \times 2)$-Cl but also on the $c(2 \times 2)$-Br phase on Cu(100) (spectrum (8) in figure 10) [33]. Although chloride and bromide form the same lateral structure on Cu(100) their charge state on Cu(100) is different. Recent *in-situ* x-ray scattering experiments point to a bromide species which is more discharged in the adsorbed state [31]. The nature of the specifically adsorbed anion has apparently no significant impact on the instantaneous reduction of adsorbed DPV on the halide-modified copper surface, at least for chloride and bromide. In full agreement with the findings of the *ex-situ* photoemission experiments are recent *in-situ* STM results on the DPV adsorption on Cu(100)-$c(2 \times 2)$-Br at high potentials which show the same $(DPV^{\bullet+}_{ads})_n$ stacking motifs as observed on the Cu(100)-$c(2 \times 2)$-Cl phase (see inset in figures 10 and 4(d)) [33].

Similar profound differences between DBV and DPV as noted for the N1s emissions are observed in the O1s spectra of the respective viologen monolayers at high potentials. Due to the absence of other oxygen containing species in the electrolyte we assign the observed O1s emissions to water. Since water tends to desorb rapidly from metal surfaces at RT under UHV conditions the O1s spectra obtained under *ex-situ* conditions cannot represent the 'pristine' state as in the electrochemical environment. However, these data can help to characterize the adsorbed viologen monolayers on a qualitative basis as being either hydrophobic or as hydrophilic.

Figure 11(a) displays the O1s region of the DBV or DPV covered electrode after emersion and transfer into UHV. It is important to note that at the used excitation energy of $E_{\text{photon}} =$ 720 eV the small peak in spectrum 2 coincides with a chloride-derived Auger transition which also contributes to the more complex spectrum 1. In order to circumvent a tedious deconvolution

of the intensity at BE higher than 534 eV in spectrum 1 into this chloride contribution and O1s components from possible water species, we base the following discussion only on the main O1s peak at BE = 532.51(2) eV in spectrum 1. This O1s binding energy is identical to that of water on the $c(2 \times 2)$-Cl/Cu(100) surface without organic adsorbates. The first observation which strikes the eye is that this peak is missing in spectrum 2. Thus, the DBV covered surface retains water after transfer into UHV, while the DPV covered surface does not; the $c(2 \times 2)$-Cl-DBV^{2+} behaves hydrophilic, the $c(2 \times 2)$-Cl-$DPV^{\bullet+}$ surface hydrophobic.

Relating the integrated intensities (I) of the N1s and the O1s emissions (corrected for the respective energy dependent cross sections (σ)) one can estimate the ratio of co-adsorbed water to di-cationic DBV^{2+}_{ads} within the 'cavitand' layer (figures 4(a) and (b) to be

$$\frac{n_{(O)}}{n_{(N)}} = \frac{I_{(O1s)}/\sigma_{(O1s)}}{I_{(N1s)}/\sigma_{(N1s)}} = \frac{2.2}{1}$$

with $\sigma_{O1s} = 0.28$ and $\sigma_{N1s} = 0.19$ at $E_{photon} = 720$ eV [32]. The ratio of water to DBV, thus, amounts to $n_{(H_2O)}/n_{(DBV)} = \frac{4.4}{1} \approx \frac{4}{1}$ considering that one viologen molecule contains 2 nitrogen atoms.

Note that this number represents only the *lower limit* of co-adsorbed water on and within the DBV^{2+}_{ads} film since a certain amount of water may yet have desorbed before the photoemission experiment was started. It should be further noted that the *lateral order* of the DBV^{2+}_{ads} film may not be conserved upon emersion out of the electrolyte phase. From adsorption phenomena of oxo-anions it is well known that the lateral order breaks down immediately when volatile co-adsorbed water species partly desorb from the electrode surface under UHV conditions. However, for the identification of the viologen redox state, whether the adsorbed species are laterally ordered or disordered does not appear crucial.

While the DBV^{2+}_{ads} monolayer has to be considered as highly hydrophilic, the compact $(DPV^{\bullet+}_{ads})_n$ phase (figure 4(c) and (d)) is hydrophobic, no water is left on the surface after emersion of the $DPV^{\bullet+}_{ads}$ covered sample (spectrum 2 in figure 11(a)). This can be seen as a further experimental hint for the presence of mono-reduced $DPV^{\bullet+}_{ads}$ species on the chloride lattice even at these high electrode potentials. The hydrophobicity of the $(DPV^{\bullet+}_{ads})_n$ monolayer is not only the result of the transition of the individual viologen di-cation to the radical mono-cation, it is also the result of the oligo- and polymerization process of individual $DPV^{\bullet+}_{ads}$ species that releases water from the surface.

All in all, the structural motifs of the viologen films observed by *in-situ* STM, the behavior of the viologen monolayers as a function of potential and the *ex-situ* XPS data point to a *non-reactive* DBV^{2+} adsorption resulting in a loosely packed and hydrophilic DBV^{2+}_{ads} film on Cu(100)-$c(2 \times 2)$-Cl, while DPV^{2+} undergoes a *reactive adsorption* at potentials more positive than the main reduction potential giving rise to the formation of a densely packed and hydrophobic $(DPV^{\bullet+}_{ads})_n$ monolayer. In this respect, the DPV behaves similarly to various di-alkylated viologens on the basal plane of HOPG [18, 19]. The characteristic pre-peaks as indicators for the reaction of the adsorbed viologen species, however, are missing in the CV of the chloride-modified Cu(100) exposed to the DPV containing electrolyte (CV 3 in figure 3). The reason for this could be the narrow potential window of copper. Note that for a bromide-modified copper surface these characteristic pre-peaks were recently observed already within the potential regime of copper dissolution and re-deposition [33].

A final topic that has to be addressed concerns a possible co-adsorption of chloride anions *within* the 2D viologen films. Both the hydrophilic DBV^{2+}_{ads} film and the hydrophobic $(DPV^{\bullet+}_{ads})_n$

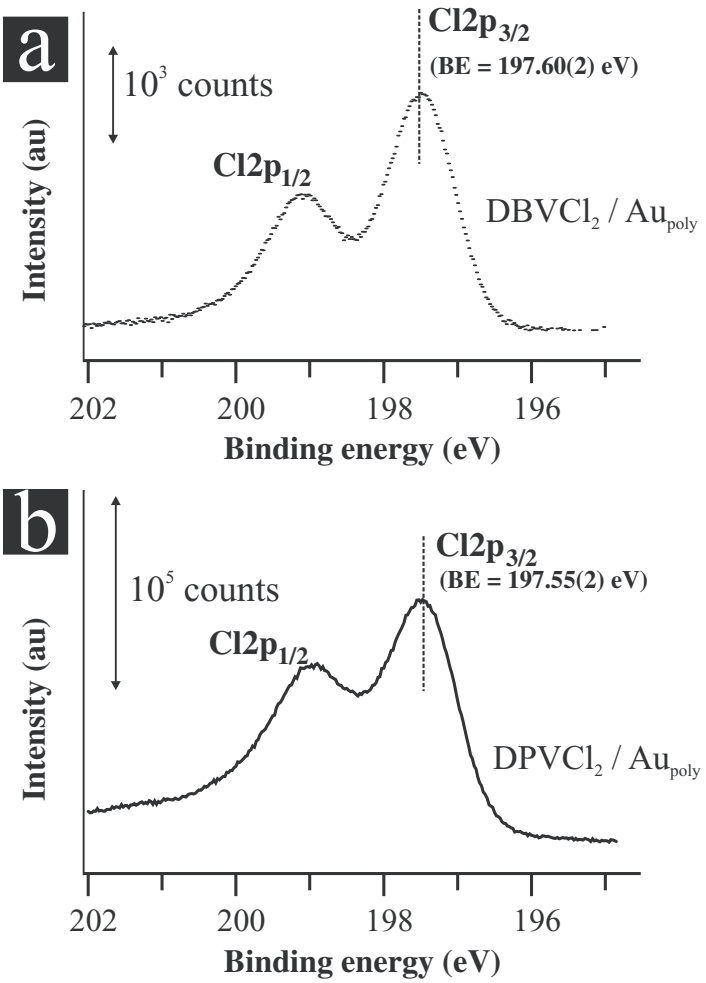

Figure 12. Cl2p photoemission spectra of the $DBVCl_2$ and $DPVCl_2$ salts deposited on inert gold foils. $E_{photon} = 720$ eV.

film are 'multi-cationic'. The main question to be answered in this context is whether further chloride anions are required to stabilize the multi-cationic 2D viologen monolayers (figure 4) besides those which are specifically adsorbed on the metallic copper.

Using the Cl2p photoemission it should be possible to differentiate between *specifically adsorbed chloride* in direct contact with the copper and additional *co-adsorbed chloride* within the viologen layer. As an internal reference, we refer to the Cl2p spectra of the $DBVCl_2$ and $DPVCl_2$ salts that were deposited on an inert gold foil (figure 12). The $Cl2p_{3/2}$ emissions of the $DBVCl_2$ and the $DPVCl_2$ di-chloride are observed at BE = 197.60(2) eV and BE = 197.55(2) eV, respectively. The chloride species within the viologen salt can be considered as ionic. For comparison, chloride species within the largely ionic CsCl salt reveals a comparably low binding energy of the $Cl2p_{3/2}$ photoelectrons of $BE_{CsCl} = 197.7$ eV [34, 35].

It can be assumed that chloride which might be co-adsorbed within the DBV^{2+}_{ads} 'cavitand' layer reveals a similar Cl2p binding energy as the one in the respective viologen salt. The Cl2p emissions obtained from the viologen-free (spectrum 1) and the viologen-covered chloride-modified electrode surfaces (spectra 2 and 3) are presented in figure 13(a). At first, one realizes

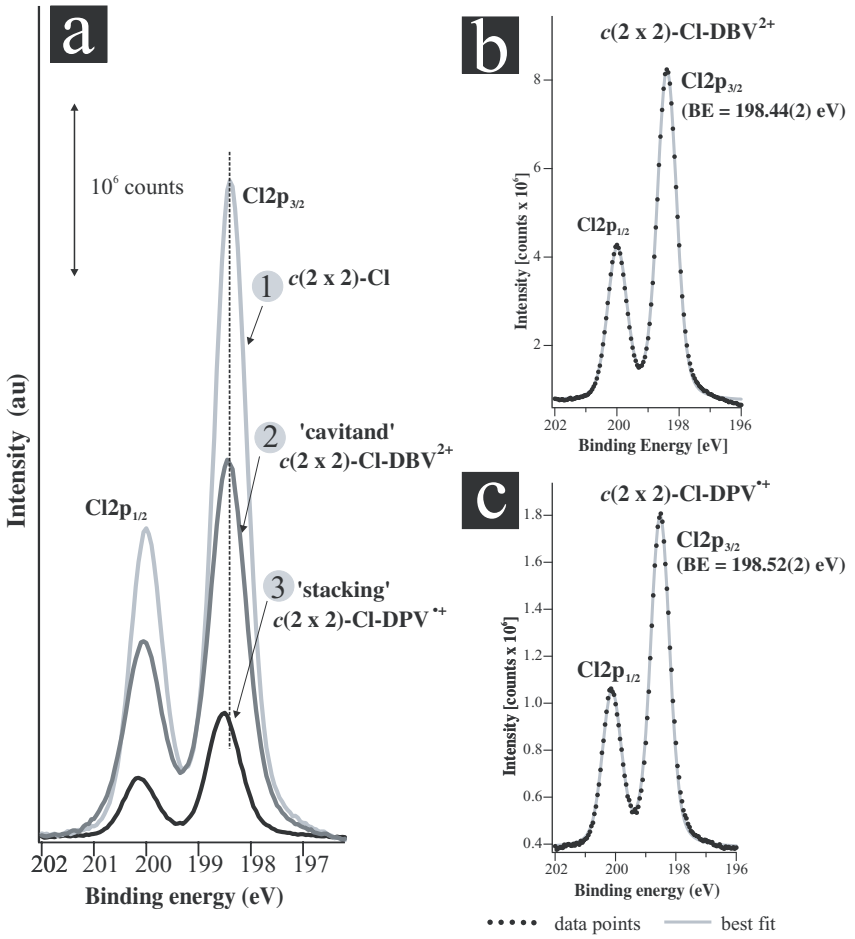

Figure 13. (a) Overview of the Cl2p photoemission spectra obtained for the viologen-free and viologen-covered Cu(100)-$c(2 \times 2)$-Cl phase, $E_{\text{photon}} = 245$ eV, (b) fitted Cl2p photoemission spectrum of the DBV^{2+}_{ads} monolayer phase; (c) Fitted Cl2p photoemission spectrum of the $(DPV^{\bullet+}_{ads})_n$ monolayer phase.

a significant decrease in intensity by going from spectrum 1 to spectrum 3. Since these spectra were obtained using an excitation energy of only $E_{\text{photon}} = 245$ eV these differences in intensity do not reflect changes in the chloride surface concentration as a consequence of the viologen adsorption but are due to 'damping' effects caused by the viologen overlayers on-top of the specifically adsorbed chloride layer. Note that at this photon energy the *kinetic* energy of the Cl2p photoelectrons ranges only from 48–43 eV. Obviously, the observed damping effect is more pronounced in case of the more compact $(DPV^{\bullet+}_{ads})_n$ stacking layer (figures 4(c) and (d)) than for the more open DBV^{2+}_{ads} 'cavitand' structure (figure 4(a) and (b)). By using higher excitation energies, e.g. $E_{\text{photon}} = 720$ eV these differences in intensity become smaller due to the increased escape depth of the photoelectrons at these higher excitation energies (data not shown here).

For the viologen-free and the viologen-covered surfaces, we find peak maxima of the $Cl2p_{3/2}$ emission at binding energies of $BE_{c(2\times2)\text{-Cl}} = 198.44(2)$ (spectrum 1), $BE_{c(2\times2)\text{-Cl–DBV}} = 198.42(2)$ (spectrum 2) and $BE_{c(2\times2)\text{-Cl-DPV}} = 198.52(2)$ (spectrum 3). While the BE of the $Cl2p_{3/2}$ photoelectrons are almost identical for the viologen-free and the chloride layer

covered with the water-containing DBV^{2+}_{ads} film there is a tiny shift of about 0.1 eV towards higher BE when the hydrophobic $(DPV^{\bullet+}_{ads})_n$ stacking layer is present. There is, however, a difference of up to $\Delta E = +0.97$ eV between the $Cl2p_{3/2}$ emission observed for the chloride anions in the viologen salts (figure 12) and the $Cl2p_{3/2}$ emissions originating from the specifically adsorbed chloride on the copper (figure 13(a)). This increase can be attributed to the specific interaction of chloride with the metallic copper substrate which involves a small partial charge transfer from the anion to the electrode. However, it should be noted that the character of the specifically adsorbed chloride remains largely ionic. For instance, the $Cl2p_{3/2}$ binding energy of the specifically adsorbed chloride on Cu(100) compares well with the $Cl2p_{3/2}$ binging energy of the ionic $NaCl_{bulk}$ salt of $BE_{NaCl} = 198.4$ eV [34, 35]. These findings agree well with recent *in-situ* x-ray diffraction studies on chloride adsorption on Cu(100) also indicating largely ionic chloride species present on the copper electrode [27].

All Cl2p spectra can be perfectly fitted by assuming only *one* chloride species (figures 13(b) and (c)), which has to be attributed to the *specifically adsorbed chloride* in direct contact with the metallic copper electrode. Further *co-adsorbed* chloride anions within the viologen film are not observed in the photoemission experiment. Obviously, additional chloride anions are not necessary to stabilize 2D viologen monolayers regardless of the particular viologen redox state. There might be a further accumulation of solvated anions on-top of the multi-cationic viologen film (see, e.g. figures 1(a)). These additional anions, however, are not transferred into the UHV in the emersion experiment. All these findings point to quite stable arrangements of these paired anion–cation layers at the interface with a clear spatial separation of negatively charged and positively charged layers (see figure 1). The presence of the cationic viologen layers does not significantly affect the copper–chloride bonding. In agreement with this there are also no chemical shifts of the copper emissions (e.g. Cu2p, Cu3p) after viologen adsorption on the chloride lattice (data not shown here). In this respect, the chloride layer can be regarded as structurally and chemically stable negative 'buffer' layer between the positive metal electrode surface and the redox-active viologen layer.

4. Conclusions

The surface redox chemistry and related phase transitions of 2D viologen monolayers were studied by means of cyclic voltammetry, *in-situ* STM and *ex-situ* photoelectron spectroscopy. Our experiments clearly indicate that there are substantial differences in reactivity of adsorbed redox-active viologens depending on the structural and electronic properties of the viologen molecules under investigation.

DBV can be regarded as prototype for a less reactive viologen species that can be adsorbed and stabilized on a halide-modified copper surface in its oxidized di-cationic form. Electrostatic attraction between the negatively charged anion layer and these di-cationic viologens are assumed to be the major driving force for their adsorption, immobilization and subsequent lateral ordering on the chloride-modified electrode surface. A reduction of DBV^{2+}_{ads} above the main redox wave does not take place. XPS data clearly indicate that di-cationic DBV^{2+}_{ads} species do not completely lose their solvation shell upon adsorption on the chloride layer. The resulting hydrophilic loosely packed 'cavitand' structure is hydrophilic and contains at least four water molecules per DBV^{2+}_{ads} molecule. Further chloride anions within the DBV^{2+}_{ads} film are not required to stabilize the viologen film. Only the specifically adsorbed chloride in direct contact with the copper electrode can be detected in the XPS experiment. It is possible to transfer the stable anion–cation layer of the specifically adsorbed chloride and the DBV di-cations into UHV.

By contrast, *DPV* can be regarded as prototype for a highly reactive viologen species. It cannot be adsorbed and stabilized in its oxidized di-cationic form on the chloride-modified electrode surface, at least within the narrow potential window of copper. Instead, DPV^{2+} instantaneously reacts to the corresponding radical mono-cation $DPV^{\bullet+}_{ads}$ at the chloride-modified surface followed by the formation of a condensed $\left(DPV^{\bullet+}_{ads}\right)_n$ π-stacked 'stripe' phase at potentials more positive than the main redox wave in the CV. This stacking layer has to be considered as highly hydrophobic which completely removes all water species from the chloride lattice. Upon adsorption and phase formation, DPV releases almost completely its solvation shell as a pre-requisite to undergoing strong inter-viologen interactions, most likely in the form of π–π interactions. These strong adsorbate–adsorbate interactions are considered as the main driving forces for the $(DPV^{\bullet+}_{ads})_n$ phase formation. The reduction and subsequent $(DPV^{\bullet+}_{ads})_n$ phase formation preferentially start at defect sites such as lower step edges and lead to an inhibition of the anodic copper dissolution. A co-adsorption of chloride anions is not required to stabilize the $(DPV^{\bullet+}_{ads})_n$ stacking layer either.

Acknowledgments

This work has been funded by the collaborative research centre 624 of the German Science Foundation and the German Federal Ministry of Research and Technology (BMBF 05 ES3XBA/5).

References

[1] Southampton Electrochemistry Group 1990 *Instrumental Methods in Electrochemistry* (Chichester: Ellis Horwood)
[2] Lustenberger P, Rohrer H, Christoph R and Siegenthaler H 1988 *J. Electroanal. Chem.* **243** 225
[3] Nyffenegger R, Gerber C and Siegenthaler H 1993 *Synth. Met.* **55–57** 402
[4] Magnussen O M 2002 *Chem. Rev.* **102** 679
[5] Frumkin A N 1933 *Z. Phys. Chem.* **A164** 121
[6] Jeong K S, Kim S Y, Shin U S, Kogej M, Hai N T M, Broekmann P, Jeong N, Kirchner B, Reiher M and Schalley C A 2005 *J. Am. Chem. Soc.* **127** 17672
[7] Pham D T, Gentz K, Zoerlein C, Hai N T M, Tsay S L, Kirchner B, Kossmann S, Wandelt K and Broekmann P 2006 *New J. Chem.* **30** 1439
[8] Pham D-T, Tsay S L, Gentz K, Zoerlein C, Kossmann S, Tsay J-S, Kirchner B, Wandelt K and Broekmann P 2007 *J. Phys. Chem.* C **111** 16428
[9] Safarowsky C, Merz L, Rang A, Broekmann P, Hermann B A and Schalley C A 2004 *Angew. Chem. Int. Ed.* **43** 1291
[10] Safarowsky C, Rang A, Schalley C A, Wandelt K and Broekmann P 2005 *Electrochim. Acta* **50** 4257
[11] Hai N T M, Wandelt K and Broekmann P 2008 *J. Phys. Chem.* C **112** 10176
[12] Bird C L and Kuhn A T 1981 *Chem. Soc. Rev.* **10** 49
[13] Monk P M S 1989 *The Viologens:Physicochemical Properties, Synthesis and Applications of the Salts of 4,4′-Bipyridines* (Chichester: Wiley)
[14] Sagara T, Fujihara T and Tada T 2005 *J. Electrochem. Soc.* **152** E239
[15] Arihara M, Kitamura F, Nukanobu K, Ohsaka T and Tokuda K 1999 *J. Electroanal. Chem.* **473** 138
[16] Mayer T, Lebedev M, Hunger R and Jaegermann W 2005 *Appl. Surf. Sci.* **252** 31
[17] Sagara T and Miuchi K 2004 *J. Electroanal. Chem.* **567** 193
[18] Sagara T, Tanaka S, Fukuoka Y and Nakashima N 2001 *Langmuir* **17** 1620
[19] Sagara T, Tanaka S, Miuchi K and Nakashima N 2002 *J. Electroanal. Chem.* **524** 68

[20] Tanaka Y and Sagara T 2007 *Electrochem. Commun.* **9** 741
[21] Kitamura F, Ohsaka T and Tokuda K 1993 *J. Electroanal. Chem.* **353** 323
[22] Kitamura F, Ohsaka T and Tokuda K 1993 *J. Electroanal. Chem.* **347** 371
[23] Wilms M, Kruft M, Bermes G and Wandelt K 1999 *Rev. Sci. Instrum.* **70** 3641
[24] Suggs D W and Bard A J 1995 *J. Phys. Chem.* **99** 8349
[25] Vogt M R, Lachenwitzer A, Magnussen O M and Behm R J 1998 *Surf. Sci.* **399** 49
[26] Vogt M R, Polewska W, Magnussen O M and Behm R J 1997 *J. Electrochem. Soc.* **144** L113
[27] Huemann S, Hai N T M, Broekmann P, Wandelt K, Zajonz H, Dosch H and Renner F 2006 *J. Phys. Chem.* B **110** 24955
[28] Safarowsky C, Wandelt K and Broekmann P 2004 *Langmuir* **20** 8261
[29] Liu X, Neoh K G, Zhao L P and Kang E T 2002 *Langmuir* **18** 2914
[30] Broekmann P, Aastasescu M, Spaenig A, Lisowski W and Wandelt K 2001 *J. Electroanal. Chem.* **500** 241
[31] Saracino M, Becker M, Gentz K, Wandelt K, Dosch H, Keller H and Broekmann P, in preparation
[32] Yeh J J and Lindau I 1985 *At. Nucl. Data Tables* **32** 1
[33] Gentz K, Wandelt K and Broekmann P, in preparation
[34] Briggs D and Seah M P 1993 *Practical Surface Analysis* (Chichester: Wiley)
[35] http://www.lasurface.com, XDB